Time-resolved fluorescence microscopy combined to Scanning ElectroChemical Microscopy (SECM): a new way to visualize photo-induced electron transfer quenching with an electrofluorochromic probe

Laetitia Guerret-Legras, Jean-Frédéric Audibert, Indra M Gonzalez Ojeda, Galina Dubacheva, Gilles Clavier, Fabien Miomandre

Time-resolved fluorescence microscopy combined to Scanning ElectroChemical Microscopy (SECM): a new way to visualize photo-induced electron transfer quenching with an electrofluorochromic probe

Laetitia Guerret-Legras, Jean-Frédéric Audibert, Indra M. Gonzalez Ojeda, Galina V. Dubacheva, Gilles Clavier and Fabien Miomandre*

PPSM – CNRS – ENS Paris-Saclay, Université Paris-Saclay, 4 avenue des Sciences, 91190 Gif/Yvette, France

Abstract

The combination of Scanning Electrochemical Microscopy (SECM) and Time-Resolved Fluorescence Microscopy was successfully implemented to investigate the control of the fluorescence of a tetrazine derivative in solution according to its redox state, a phenomenon called electrofluorochromism. The normalized fluorescence intensity difference between the 'on' and 'off' states can be tuned by the tip potential and the distance between the polarized tip and the substrate. It is demonstrated for the first time that luminescence lifetime can be modulated as well, an evidence that a quenching process contributes to the fluorescence intensity drop. The experimental results demonstrate that this quenching is due to the electron transfer reaction between the excited fluorophore and the electrogenerated anion radical. A mixed dynamic and static quenching mechanism is considered to fit the variations of both luminescence intensity and lifetime ratios vs. the coulombic charge. The pertinence of a static quenching is validated by DFT calculations. Insulating (glass) and conductive (ITO) substrates have been tested and optical approach curves based on fluorescence lifetime modulation have been obtained in each case that are more sensitive than the electrochemical one based on the tip current. Finally, numerical simulations have been performed to fit these optical approach curves and validate the role of the electron transfer quenching in the variation of fluorescence intensity and lifetime.

Keywords: Time-resolved fluorescence; electrofluorochromism; SECM; tetrazine; quenching

1. Introduction

Fluorescence microscopy is a well-known imaging technique widely used to investigate chemical or biochemical events. Its advantages rely on its high sensitivity and its ability to localize events at very short scales using for example confocal[1] or TIRF[2] configuration. Its coupling with electrochemistry is now well documented in the literature[3-7] and even compact all-in-one devices now allow the simultaneous record of fluorescence and electrochemical signals through voltafluorograms or chronofluoamperograms[8]. Electrochemistry can be coupled to fluorescence for various aims: as a trigger or as a complementary detection technique. The simplest

configuration to do this is to use the substrate (microscope slide or coverslip) as the working electrode in a three electrode electrochemical cell[9]. This requires the substrate to be both transparent and conductive enough with generally a trade-off between the optical and electrochemical performances. Another way of using an electrochemical input signal with fluorescence microscopy is through an ultramicroelectrode (UME) tip scanning the substrate surface, the typical configuration of Scanning ElectroChemical Microscopy (SECM)[10-11]. In that case, microscope glass coverslips can be used as substrates without any need of making them conductive because the electrochemical addressing can be made by the tip. This concept was already implemented by Bard et al. to combine SECM and Electrochemiluminescence (ECL) in a single experiment.[12-14] Using fluorescence instead of ECL broadens the scope of the possible emitters to be used, with high luminescence yield and no need of coreactant.

A few examples combining SECM and fluorescence microscopy in a single experiment have been reported[15,16] and recently applied to the investigation of biochemical events like the detection of ROS in human cells[17] or ion permeation through nuclear pore complex[18] but also to the analysis of nanometer-size defects in insulating layers[19]. On our side we demonstrated the possibility to couple these two techniques using a single moiety as the redox fluorogenic probe either in organic[20] or in aqueous[21] medium. In these recent papers, we showed that various SECM modes (positive and negative feedback, generation-collection) could be coupled to epifluorescence microscopy in wide field to control the fluorescence state of the probe and obtain optical approach curves complementary to the electrochemical ones. The optical output signal was the luminescence intensity extracted from the CCD camera and the emission spectrum. Another valuable source of information can be obtained through luminescence lifetimes when pulse excitation is used. Fluorescence lifetime imaging microscopy (FLIM) is a widespread technique in the investigation of biological and biomedical issues[22,23]. Performing FLIM under an electrochemical control is an innovative technique that might find valuable developments in all biological issues where redox states of cells need to be determined which is precisely done by fluorescence measurements[24,25].

We already reported before the possibility of using time-resolved fluorescence microscopy combined with electrochemistry [26,27] and it was shown that the luminescence lifetime was electrochemically modulated as the emission intensity was, highlighting the role of the electrogenerated species in the quenching mechanism. However, the electrochemical control of luminescence lifetime, although highlighted a long time ago in the case of ruthenium complexes[28] has not been exploited so far as an analytical tool. We were interested in going further in this investigation and for that we implemented a pulsed laser source on the combined SECM-fluorescence microscope setup, allowing us to perform for the first time **time-resolved fluorescence microscopy coupled to SECM**. As the laser source we used delivers sub-nanosecond pulses, it is better suited to measure long luminescent lifetimes. Among electrofluorochromic probes available, tetrazines are organic molecules with outstanding long lifetimes in the range of 10 to more than 100 ns[29]. Therefore, we decided to focus our study on chloromethoxy-1,2,4,5-tetrazine (see scheme 1). This molecule is used as the redox fluorescent reporter and is particularly suited for this kind of measurement due its relatively high reduction potential (-0.99 V vs. Fc), electrochemical reversibility ensuring anion radical stability, high emission quantum yield (0.38) and very long lifetime (160 ns),[30] one of the highest among the tetrazine derivatives. The mechanism is investigated through the thorough analysis of lifetime evolution with the potential applied at the tip and when varying the tip-

substrate distance. In the latter case, optical approach curves are obtained and analyzed through Comsol™ modelling. The results are analyzed successively for an insulating (glass) or a conductive (ITO) substrate.

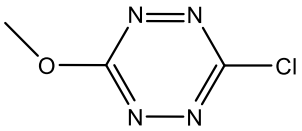

Scheme 1 : Formula of chloromethoxy-1,2,4,5-tetrazine

2. Experimental

Chemicals. Chloromethoxytetrazine was synthesized according to a previous report[27] and then dissolved in acetonitrile (Spectro. Grade, SDS) in presence of tetrabutylammonium hexafluorophosphate (puriss. from Fluka) 0.1 M. The approximate concentration of tetrazine is 1 mM. The solution is deaerated by argon bubbling.

DFT calculations. Three dimers were considered: two neutral tetrazines, one neutral and one reduced (radical anion) tetrazines and two reduced tetrazines (anion radicals). Their geometry was optimized at the APFD/6-31+g(d) level of theory with and without BSSE correction. The latest did not change the resulting geometry. A frequency calculation was done to confirm that a minimum was obtained. APFD was chosen because it includes empirical dispersion that is beneficial for modeling intermolecular interactions. Finally energy calculations were done at the APFD/6-311++g(d,p) and ωB97X-D/6-311++g(d,p) levels of theory with BSSE correction to estimate the complexation energy. The ωB97X-D hybrid long-range corrected functional was specifically designed to study non-bonded interactions. All calculations were done with Gaussian 16 (Revision B.01)[31].

Electrochemical measurements. All electrochemical and SECM measurements were performed at room temperature using a homemade three-electrode cell on top of an inverted optical microscope (see below). A platinum wire and a Ag wire were used as counter and pseudo-reference electrode respectively. Glass (purchased from VWR, 1 mm thickness) and ITO (purchased from Solems, 25-35 ohm.□, 80 nm ITO thickness on glass) coverslips were employed as the substrates and working electrode in the case of ITO. A ultramicroelectrode (UME) made of a 25 µm diameter platinum disk (purchased from Ametek) was used as the tip and second working electrode and positioned above the substrate thanks to a mechanic arm connected to a piezo positioner (VersaSCAN motion controller) which enables to control the tip position under VersaSCAN Software. All electrochemical measurements are performed after 5 minutes of argon bubbling, so that dissolved oxygen has been removed.

Optical set-up. Optical measurements were performed on an inverted microscope (Ti Eclipse Nikon) with a 40X NA 0.75 objective in a wide field epi-illumination. Chloromethoxytetrazine was excited by a Hg lamp (C-HGFI - Intensilight, Nikon) with an excitation filter (BP482 nm) or a pulsed laser diode at 470 nm (LDH-P-C-470, Picoquant) with pulse width of 30 ps and a repetition rate of 2.5 MHz. Emitted light is collected through a long

pass emission filter (LP 520 nm). Acquisition time-lapses are carried out using a CCD Pixel Fly camera from PCO at 14.2 images/s under the µManager open source software for steady state measurements. Fluorescence intensity over time is reported as the mean intensity inside a square region of interest (ROI) of the total image centered on the tip (wide field configuration). Photon counting over time is done using a graded index multimode fiber APD (MPD-CCTC, Picoquant) with a mode field diameter of 60 µm in sample plane for time resolved measurement and analyzed with homemade script and broad numerical methods under Igor Pro Wavemetrics Inc. software.

Fluorescence lifetime and intensity measurements. The general principle is based on Time-Correlated Single Photon Counting (TCSPC), a technique which was already performed under voltage bias[32]. In our investigation photons are recorded in TTTR (Time-Tagged Time resolved) mode[33] at 2.5MHz with a TCSPC 260Nano PCIe card from Picoquant with a global IRF resolution of 550 ps FWHM. The discrete intensity average lifetime for a sampling period j over the total acquisition time is estimated from the number n_i of photons emitted after a dt_i delay-time respect to the pulse excitation for each channel i, according to the following equation:

$$\tau_j = \frac{\sum_i n_i \cdot dt_i}{\sum_i n_i}$$

Only the number of photons over a certain threshold (corresponding to the experimental dark current of the detector) are counted. Since in TTTR mode absolute arrival time and delay for each photon are processed, intensity over time and decay for a specific period can be extracted and analyzed (Figure SI-1). Intensity average lifetime for a simple exponential decay was estimated by nonlinear least square Lenvenberg-Marquardt[34], Maximum-Likelihood Estimator[35] method and compared with discrete intensity average lifetime method (Figure SI-2). According to the experimental parameters and the number of the collected photons over a same period, the expected accuracy for mono exponential lifetimes ranging from 25 ns to 160 ns estimated by weighted least-squares method is 0.95% and 0.45% respectively[36].

The global setup can be represented in scheme 2. The substrate and UME tip can be polarized separately with the bipotentiostat. The two microscope outputs are the CCD camera for image and intensity recording on one hand and APD for lifetime measurement on the other hand.

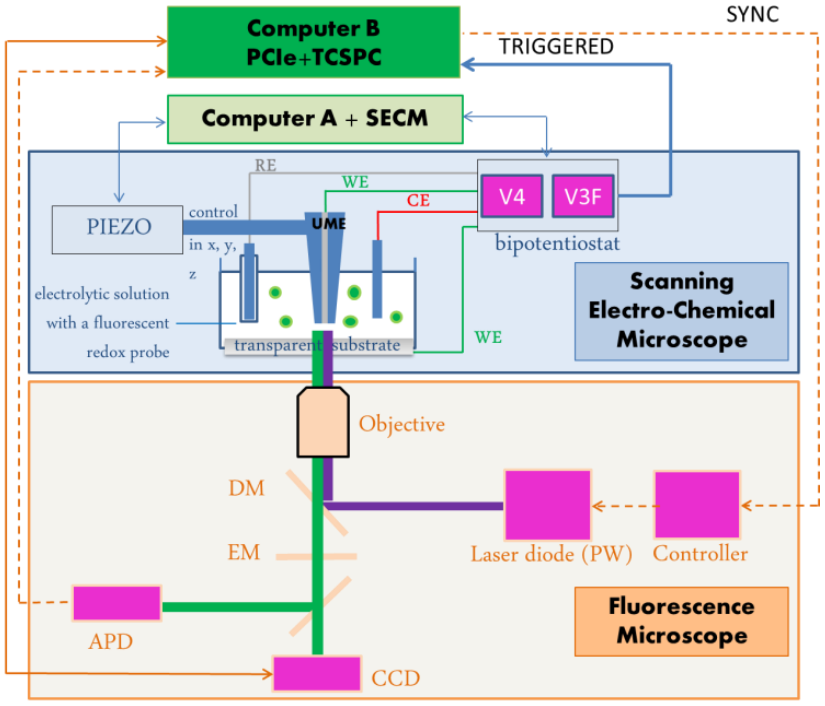

Scheme 2. Time-resolved fluorescence microscope (bottom, orange part) combined with Scanning Electrochemical microscope (top, blue part). DM = dichroic mirror. EM = emission filter. APD= Avalanche PhotoDiode. RE = Reference electrode. CE = counter electrode. WE = working electrode. UME = Ultramicroelectrode. TCSPC = Time Correlated Single Photon Counting.

In this paper, two kinds of experiments are performed:

- Application of a sequence of various potential at fixed position of the tip
- Variation of the tip position for a given sequence of potential

The first part allows us to investigate the mechanism of quenching by analyzing the modulation of the emission lifetimes induced by the potential signal at the tip (and possibly at the substrate if conducting). This can be used in the second part to reconstruct the optical approach curve (luminescence intensity vs. tip-substrate distance) and explain its better sensitivity compared to the electrochemical approach curve. Finally Comsol™ simulation is performed to try to fit the experimental data with the best accuracy.

3. Results and discussion

3.1 SECM-time resolved fluorescence experiments on insulating substrate

The first experiment conducted was done on insulating substrate (glass) at a fixed position of the UME tip above the substrate. The tip-substrate distance is chosen equal to 30 µm, a value close to the tip diameter so that the tip is sensitive to what happens on the substrate. First, a cyclic voltammogram is recorded on the Pt tip (see

figure 1) to determine the potential range where the reduction of chloromethoxytetrazine takes place. The classical waveform signal expected for a microelectrode scanned at low scan rate is actually visible. The half-wave potential can be estimated to -0.55 V vs. the pseudoreference used.

The substrate being insulating, the electrochemical monitoring signal was applied at the tip and consists (after a 10 s period under open circuit) of a double potential step from a value where the EFC probe is in its emissive form (typically 0 V) to progressively more negative values starting from -0.4 V to gradually induce luminescence quenching. The potential is finally stepped back to its initial value to check the reversibility. The results can be seen in figure 1 where the electrochemical current (1A), luminescence intensity (1B) and lifetime (1C) are simultaneously recorded and displayed as functions of time. When more and more negative potential values are applied at the tip, the fluorescence intensity drops more and more dramatically as expected, while the current gets larger in intensity. Interestingly the luminescence lifetime follows the same trend as the luminescence intensity, getting also smaller as the intensity decreases. This is indicative of a quenching mechanism, becoming more pronounced as the potential is more negative. Therefore, it can be confirmed that the fluorescence intensity drop is not only due to the disappearance of fluorophores induced by the electrochemical reaction, but also to a chemical reaction between the remaining fluorophores and a quencher. We can suppose that in absence of dissolved oxygen the main quencher is the electrogenerated species (tetrazine anion radical) but this must be quantitatively analyzed, especially by correlating the intensity and lifetime ratios (in absence vs. in presence of quencher) to the injected charge during the electrochemical process. These three parameters can be experimentally extracted for each potential value (figure 2A) and finally the two ratios plotted against the coulombic charge (figure 2B).

These two ratios increase with the injected charge as expected, meaning that quenching becomes more efficient as the electrochemical reaction goes forward. At first sight, the lifetime ratio seems to vary linearly with the coulombic charge, which fits the Stern-Volmer quenching model.

Indeed, according to this model the following equation (1a) should be valid:

$$\frac{I_0}{I} = \frac{\tau_0}{\tau} = 1 + K_{SV}[Q] = 1 + K_{SV}\frac{C}{FV} \qquad (1a)$$

With: I_0 , I : steady-state emission intensities resp. in absence and in presence of quencher

τ_0 , τ: emission lifetimes resp. in absence and in presence of quencher

$K_{SV} = k_Q\tau_0$: Stern-Volmer constant (k_Q : quenching rate constant).

C = coulombic charge injected during the electrochemical reaction

F = Faraday constant (F = 96500 C mol^{-1})

V= volume of solution probed.

The probed volume can be estimated according to the tip position z by:

$$V = \frac{\pi}{4} w^2 z \quad (1b)$$

where w is the Gaussian beam diameter measured at $1/e^2$ (typically 40 µm in our case).

Equation (1a), which combines Stern-Volmer relation and Faraday's law applies if only dynamic quenching is involved, that is if the quenching process involves the mutual diffusion of the emitter and the quencher, without any additional process.

The coulombic charge can be estimated by integrating the transient current on the time interval T necessary to establish the steady state diffusion of the reactant. It can be expressed as a function of electrode potential using Cottrell equation[37]:

$$C(E) = \int_0^T i dt = \int_0^T 4\pi {r_0}^2 DF[c_{bulk} - c(E)] \left(\frac{1}{\sqrt{\pi D t}} + \frac{1}{r_0}\right) dt = 2 r_0 \frac{I_{stat}(E)}{\sqrt{\pi D}} \sqrt{T} \quad (2)$$

$$\text{with} \qquad I_{stat}(E) = 4\pi r_0 DF[c_{bulk} - c(E)]$$

where r_0 is the electrode radius, D is the diffusion coefficient, c_{bulk} is the bulk concentration of reactant and $c_{(E)}$ is the concentration of reactant at the electrode polarized at potential E. I_{stat} is the stationary current at the tip considered as a UME.

From the combination of (1) and (2), we can draw the equation for the variation of the charge, emission intensity and lifetime ratios with the potential. Then both ratios can be plotted vs. the coulombic charge. The results are shown in figure 2 (full lines) where they are compared with experimental data.

As expected, the charge, emission intensity and fluorescence lifetime ratios all increase as the potential is more negative. Moreover, a linear relationship for the lifetime ratio vs. charge is actually obtained, in agreement with the Stern-Volmer model. The linear fit leads to an estimation of the quenching rate constant k_Q of 5.8 10^9 $Lmol^{-1}s^{-1}$, (see table 1), which is very close to the value predicted by Smoluchowski equation[38] for diffusion-limited bimolecular reactions assuming D equal to 10^{-5} $cm^2 s^{-1}$ and a distance between reactants of 1 nm.

However, in Stern-Volmer model the steady-state intensity ratio is supposed to vary linearly with the charge as the lifetime ratio, which is not the case according to figure 2. Therefore, a more complicated quenching mechanism must be envisioned. We may consider adding a static quenching, i.e. the possibility that a quencher may quench all the fluorophores in a given volume around it without necessity of mutual diffusion.

A combined dynamic and static quenching model leads to the following equation (3):

$$\frac{I_0}{I} = (1 + K_{SV}[Q])(1 + K_S[Q]) = \frac{\tau_0}{\tau}(1 + \frac{K_S}{VF} C) \qquad (3)$$

where K_s is the equilibrium constant for the formation of the complex between the emitter (in the fundamental state) and the quencher.

In that model, the lifetime ratio still varies linearly with the quencher concentration as previously, because only the intensity ratio is affected. If that model is valid, a quadratic relationship should appear between the intensity ratio and the injected charge C:

$$\frac{I_0}{I} = 1 + (K_{SV} + K_s)[Q] + K_{SV}K_s[Q]^2 = 1 + \frac{K_{SV}+K_s}{VF}C + \frac{K_{SV}K_s}{(VF)^2}C^2 \qquad (4)$$

Therefore, we proposed a quadratic function to fit the experimental data (figure 2, bottom panel). A good fit is observed demonstrating that the model is relevant. Numerical values for K_{SV} and K_s can be deduced from the combination of a linear fit for lifetime ratio (giving K_{SV} through equation (1)) and a quadratic fit for intensity ratio (giving K_s knowing K_{SV} using equation (4)).

The results are listed in table 1. The values have the order of magnitude expected for a very efficient quenching process[39].

Table 1: Quenching rate constant, Stern-Volmer and static quenching constants for the various substrates extracted from experimental data.

Substrate	k_Q (10^9 L mol^{-1} s^{-1})	K_{SV}(L mol^{-1})	K_s(L mol^{-1})
glass	5.8	760	480
ITO polarized at -0.23V	4.9	637	-
ITO at open circuit	2.2	286	-

To go further, the authenticity of this additional static quenching assumption has been checked by computational chemistry. DFT calculations have been implemented to assess the interaction between a neutral *s*-tetrazine and its anion radical by evaluating the stability of a complex between these two moieties.

Three possible tetrazine-tetrazine complexes were studied: the two neutral, one neutral and one reduced (anion radical) and the two anion radicals. In the case of two anion radicals, no calculation method and relative orientations of the two aromatics did converge toward a stable geometry. It was thus concluded that the interaction between two tetrazine anion radicals is unfavorable. Conversely, stable complexes could be obtained for the two other cases. Table 2 shows the complexation energy values obtained by applying the basis set superposition error (BSSE) correction method. Whatever the calculation method, the value is negative, demonstrating that this interaction is favorable. Moreover, the values are more negative for the mixed Tz,Tz$^{\bullet-}$ complex than in the case of the supramolecular interaction between two neutral Tz.

Table 2 : Energy (kcal mol^{-1}) calculated for the complexes formed by the interaction between two neutral tetrazines (Tz,Tz) or one neutral tetrazine and its anion radical (Tz,Tz$^{\bullet-}$).

Method	(Tz,Tz)	(Tz,Tz$^{\bullet-}$)
ωB97X-D	-7.47	-14.97
APFD	-8.07	-25.43

Molecular orbitals (MOs) and spin density for the supramolecular system (Tz,$Tz^{\bullet-}$) are represented in figure 3. One can notice that MOs lost their molecular character with a contribution spread on the two units. In particular, the SOMO is highly delocalized and the spin density is especially high in the interspace. These two factors demonstrate that a close interaction is possible between Tz and $Tz^{\bullet-}$, making the static quenching of Tz^{*} by $Tz^{\bullet-}$ likely to occur.

Another experiment is performed by moving the tip polarized at a fixed potential (allowing the tetrazine reduction) in the vertical direction *z*. This consists in the typical approach curve which is systematically used to position the tip at the closest distance of the substrate surface before scanning it for analysis. The results obtained at various tip positions are shown in figure 4. The electrochemical current (top panel) varies consistently with a negative feedback mode, that is the current drops as the tip approaches the surface, as expected for an insulating substrate. As the tip gets closer to the surface, the emission intensity displays a gradual decrease in the 'on' state because the probed volume gets smaller as well as a modulation in the 'off' state, which has been analyzed in detail in a previous publication[20]. The normalized difference between these 'on' and 'off' intensities $(I_{on}-I_{off})/I_{on}$, which can be considered as the normalized optical contrast, can be plotted as a function of the tip-substrate distance and shows a gradual increase when the gap shortens. This constitutes the optical approach curve (green curve, top panel in figure 4) as already defined in a previous paper[20]. Finally, a similar behavior is also observed for the normalized difference of emission lifetimes $(\tau_{on}-\tau_{off})/\tau_{on}$ when this factor is plotted vs. the tip-substrate distance[1] (blue curve), which is a new result.

[1] the point at closest distance should be considered with care as lifetime is extracted from a very low intensity.

This variation of the lifetime modulation amplitude with the tip position is an indication that quenching plays a role in the optical approach curve based on the luminescence intensity. This will be analyzed in more details below.

Interestingly the lifetime and intensity modulation amplitudes vary more significantly at large tip-substrate distances than the electrochemical current does. This is because the electrochemical current is sensitive to diffusion processes and the presence of a boundary (substrate) does not change the diffusion rate until very short distances are reached. The optical signal is not only influenced by diffusion but also by the quenching mechanism as suggested above and demonstrated further. Globally the variation of fluorescence intensity and lifetime vs. distance shows a variation spreading over 200 µm, while the electrochemical current starts to vary only below 100 µm.

3.2 SECM-time resolved fluorescence measurements on conductive substrates

Similar measurements have been performed on a conductive substrate (ITO). When ITO is left under open circuit conditions, a positive feedback is expected like already demonstrated in our previous work[20]. When polarized at a potential where no reoxidation of the anion radical is possible (−0.23 V), this positive feedback is not possible anymore. Figure 5 shows the results obtained for these two situations. For both, when the tip potential is stepped to more and more negative values, the electrochemical current increases (in absolute value) while the fluorescence intensity and fluorescence lifetimes drop. When comparing more closely figures 5A and 5B, it can be seen that the lifetime modulation is deeper in the case of polarized ITO than for ITO left at open circuit. Indeed, in the first case the anion radical can not be reoxidized on the substrate, so that the amount of quencher is higher and therefore the lifetime is shorter, the other parameters (tip potential, tip-substrate distance) being kept constant.

As in the previous section for insulating substrate, the variation of fluorescence lifetime and fluorescence intensity ratios are plotted against the coulombic charge (see figure 6). Linear fitting works well for the lifetime ratio as it did previously for the insulating substrate, but leads to lower slopes, which corresponds to smaller values for the Stern-Volmer constant. This is consistent with the fact that the quenching is less efficient, because the anion radical quencher has been partly reoxidized on the substrate. Polarizing ITO to a value inhibiting the reoxidation of the anion radical leads to a situation close the one of the glass substrate, meaning that a negative feedback occurs on the substrate under this polarization value. All these results tend to demonstrate that the anion radical produced actually acts as a quencher of the luminescence emission and its amount can be tuned depending on the substrate nature and polarization.

3.3 Optical approach curves modelling

The tip-substrate space and the region of interest (ROI) where the fluorescence is collected are represented in scheme 3:

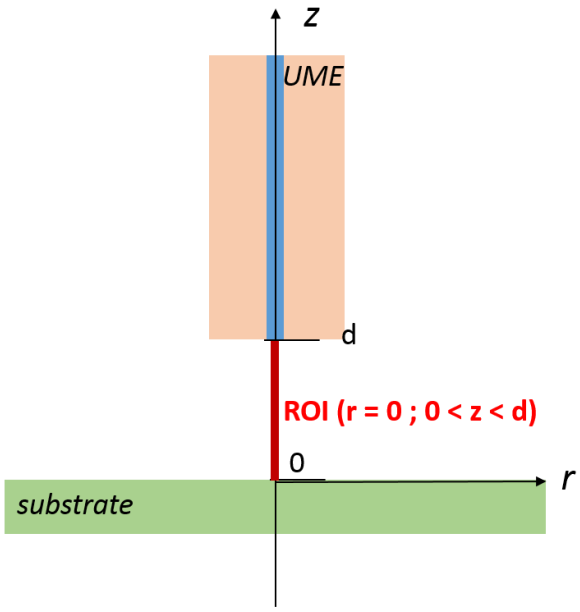

Scheme 3: Geometry of the tip-substrate space used in the Comsol™ modelling. The region of interest (ROI) is the space where the emission is collected (shown in red). The conductive part of the ultramicroelectrode (UME) tip of diameter d is shown in blue.

We previously reported a modelling of the SECM – fluorescence coupling by finite element method enabling to calculate the concentration fields of neutral and electrogenerated radical anion of tetrazine, respectively [Tz](r,z) and [$Tz^{\bullet-}$](r,z) for each tip-substrate distance[20]. This modelling considered the fluorescence intensity collected in a fictive ROI as directly proportional to the number of emitting species in this ROI. Nevertheless, such an assumption was unable to explain the better sensitivity of the optical approach curves compared to the electrochemical ones. So we decided to refine the model by taking into account the quenching mechanism mentioned above.

For this purpose, we use the local expression of the fluorescence intensity derived from Beer-Lambert law:

$$dI_{kq}(r=0,z) = \epsilon\, \varphi_{kq}(r=0,z) I_0 [Tz](r=0,z) \ln(10) \qquad (5)$$

Where ϵ is the extinction coefficient and $\varphi_{kq}(r=0,z)$ is a local quantum yield :

$$\varphi_{kq}(r=0,z) = \frac{k_r}{k_r + k_{nr} + k_q [Tz^{\bullet-}](r=0,z)} \qquad (6)$$

In equation (6) k_r and k_{nr} are the radiative and non-radiative constants respectively. It states that the excite state may evolve by either radiative pathways (luminescence), or non-radiative pathways among which the quenching by electron transfer with the electrogenerated anion radical produced at the tip (r= 0).

For each tip-substrate distance d, the fluorescence intensity collected in the ROI is obtained by integration of the local one between z=0 and z=d. This leads to the following expressions for the intensities with and without electrochemical reaction at the tip, I_{min} and I_{max} respectively:

$$I_{min,kq}(d) = \epsilon\, I_0 \ln(10) \int_0^d \frac{k_r}{k_r + k_{nr} + k_q[Tz^{\bullet-}](r=0,z)} [Tz](r=0,z)dz \qquad (7)$$

$$I_{max,kq}(d) = \epsilon\, I_0 \ln(10) \int_0^d \frac{k_r}{k_r + k_{nr}} [Tz]_0 dz = \epsilon\, I_0 \ln(10)\, \frac{k_r}{k_r + k_{nr}} [Tz]_0 d \qquad (8)$$

Equation (7) clearly shows that $I_{min}(d)$ is not directly proportional to the number of emitters in the ROI when considering an inhomogeneous quantum yield.

The normalized fluorescence intensity modulation is then obtained for each tip-substrate distance by calculating the following expression:

$$I.M._{.kq}\,(d) = \frac{I_{max}(d) - I_{min}(d)}{I_{max}(d)} \qquad (9)$$

Comsol™ is used to evaluate the value of the integral in equation (7) thanks to experimental values of k_r and k_{nr}, and then to calculate a theoretical optical approach curve using equation (9).

Such a curve can be simulated for various values of the k_q parameter, from 0 in the absence of quenching to about 10^{10} for a diffusion-limited quenching reaction.

The modelling results are reported in Figure 7A. It can be seen that the variation of the modulation spreads over a larger distance as the quenching rate constant is higher: as expected, the more efficient the quenching is, the better the sensitivity of the simulated approach curves. Nevertheless, the behavior of the modelling curves differs from the experimental ones for the long tip-substrate distances. This is probably due to optical effects in the experiment, as differences were observed according to the excitation source (laser or white lamp). Indeed, the tip looks more and more tiny in the ROI of constant size when the tip-substrate distance increases. Probably, modelling results could also be improved by considering a local quenching constant $k_q(r,z)$ depending on the location instead of a global one.

Beyond the fluorescence intensity, it is interesting to model the lifetime as well. For this purpose the Stern-Volmer relation was used in which emission lifetime is related to the quencher concentration [$Tz^{\bullet-}$]. A mean lifetime is thus calculated for each tip-substrate distance d after calculation of the mean anion radical concentration in the ROI :

$$[Tz^{\bullet-}]_{ROI,d} = \frac{1}{d} \int_0^d [Tz^{\bullet-}](r=0,z)dz \qquad (10)$$

The lifetime based optical approach curve is finally obtained by calculating the normalized amplitude modulation:

$$\tau_{M,kq}(d) = \frac{\tau_0(d) - \tau_{kq}(d)}{\tau_0(d)} \qquad (11)$$

As for fluorescence intensity, k_q is used as a parameter and an optical approach curve is calculated for each value (figure 7B).

As expected, a strong dependence of the k_q value is observed on the curve shape. For short tip-substrate distances, the model matches pretty well with experimental data considering the highest quenching rate constant values, corresponding to a diffusion-limited reaction, up to 100 µm. At longer tip-substrate distances, a gap between the modelling and the experimental curves appears, because the model is probably limited by the fact that mean values are considered and the same optical effects as previously mentioned should also explain the differences observed.

4. Conclusion

SECM was successfully combined with time-resolved fluorescence microscopy in a single experiment for the first time, with chloromethoxytetrazine as the redox-active fluorescent probe. Compared to our previous works, we show that luminescence lifetime, as luminescence intensity, is modulated according to the tip potential and tip-substrate distance. This shows that the luminescence intensity drop is not only due to the disappearance of the emitter due to the electrochemical reaction, but also to a quenching reaction, involving the electrogenerated anion radical. The quenching mechanism is a mix of dynamic and static quenching since the variation of intensity ratio (in presence vs. in absence of quencher) vs. coulombic charge cannot be fitted by a linear variation. A similar behavior is observed whatever the substrate nature (insulating or conducting), but when a positive feedback occurs on the substrate, the lifetime drop is deeper. Polarizing the ITO substrate at a value inhibits the positive feedback and this can be seen directly on the variation of both fluorescence intensity and fluorescence lifetime. Finally, approach curves based on the variation of fluorescence lifetime with the tip-substrate distance can be constructed with a variation spreading over much larger distance values than the electrochemical current. This better sensitivity is explained by the participation of quenching in the luminescence modulation, as demonstrated by a Comsol™ modelling where the effect of the quenching rate constant on the approach curves is clearly established.

This unique combination of time-resolved fluorescence and electrochemical microscopies allows one to image how the luminescence lifetime varies upon an electrochemical reaction and thus gives direct evidence of electron transfer reactions involving the excited state of a molecule with the reduced form of it. FLIM measurements under electrochemical control can be envisaged with a tunable ROI controlled by the tip-substrate distance. This should open new routes for the investigation of chemical or biochemical processes occurring on the substrate.

Acknowledgments

CHARMMMAT Labex (ANR-11-LABX-0039) and Region Ile-de-France (C'Nano network) are acknowledged for financial support.

The University of Michigan, promotor of the program 'Optics in the city of lights' is acknowledged for funding the internship of I.M. Gonzalez Ojeda.

This work was granted access to the HPC resources of CINES under the allocation 2018-A0050810547 made by GENCI and HPC resources from the “Mésocentre” computing center of CentraleSupélec and École Normale Supérieure Paris-Saclay supported by CNRS and Région Île-de-France (http://mesocentre.centralesupelec.fr/) for DFT calculations.

References

1. H. Shuman, J. M. Murray and C. Dilullo, Confocal microscopy: an overview. *Biotechniques*, **1989**, *7*, 154-&.
2. A. Trache and G. A. Meininger, Total internal reflection fluorescence (TIRF) microscopy, *Curr. Protoc. Microbiol.*, **2008**, Chapter 2, Unit 2A.2.1-2A.2.22.
3. Dias, M.; Hudhomme, P.; Levillain, E.; Perrin, L.; Sahin, Y.; Sauvage, F. X.; Wartelle, C., Electrochemistry coupled to fluorescence spectroscopy: a new versatile approach. *Electrochem. Commun.* **2004,** *6*, 325-330.
4. Loete, F.; Vuillemin, B.; Oltra, R.; Chaumont, D.; Bourillot, E., Application of total internal reflexion fluorescence microscopy for studying pH changes in an occluded electrochemical cell: Development of a waveguide sensor. *Electrochem. Commun.* **2006,** *8* (6), 1016-1020.
5. Lei, C.; Hu, D.; Ackerman, E. J., Single molecule fluorescence spectroelectrochemistry of cresyl violet. *Chem. Commun.* **2008**, 5490-5492.
6. P. Audebert and F. Miomandre, Electrofluorochromism: from molecular systems to set-up and display. *Chem. Sci.*, **2013**, *4*, 575-584.
7. C. Amatore, S. Arbault, Y. Chen, C. Crozatier, F. Lemaitre and Y. Verchier, Coupling of electrochemistry and fluorescence microscopy at indium tin oxide microelectrodes for the analysis of single exocytotic events. *Angew. Chem. Int. Ed.*, **2006**, *45*, 4000-4003.
8. D. Martin-Yerga, A. Perez-Junquera, D. Hernandez-Santos and P. Fanjul-Bolado, Time-Resolved Luminescence Spectroelectrochemistry at Screen-Printed Electrodes: Following the Redox-Dependent Fluorescence of $Ru(bpy)_3^{2+}$. *Anal. Chem.*, **2017**, *89*, 10649-10654.
9. F. Miomandre, R. Meallet-Renault, J.-J. Vachon, R. B. Pansu and P. Audebert, Fluorescence microscopy coupled to electrochemistry: A powerful tool for the controlled electrochemical switch of fluorescent molecules. *Chem. Commun.*, **2008**, 1913-1915.
10. A. J. Bard, M. V. Mirkin, P. R. Unwin and D. O. Wipf, SCANNING ELECTROCHEMICAL MICROSCOPY .12. THEORY AND EXPERIMENT OF THE FEEDBACK MODE WITH FINITE HETEROGENEOUS ELECTRON-TRANSFER KINETICS AND ARBITRARY SUBSTRATE SIZE. *J. Phys. Chem.*, **1992**, *96*, 1861-1868.
11. H. Y. Liu, F. R. F. Fan, C. W. Lin and A. J. Bard, SCANNING ELECTROCHEMICAL AND TUNNELING ULTRAMICROELECTRODE MICROSCOPE FOR HIGH-RESOLUTION EXAMINATION OF ELECTRODE SURFACES IN SOLUTION. *J. Am. Chem. Soc.*, **1986**, *108*, 3838-3839.
12. Fan, F. R. F.; Cliffel, D.; Bard, A. J., Scanning Electrochemical Microscopy. 37. Light Emission by Electrogenerated Chemiluminescence at Secm Tips and Their Application to Scanning Optical Microscopy. *Analytical Chemistry* **1998**, *70*, 2941-2948.
13. Miao, W. J.; Choi, J. P.; Bard, A. J., Electrogenerated Chemiluminescence 69: The Tris(2,2 '-Bipyridine)Ruthenium(Ii), (Ru(Bpy)(3)(2+))/Tri-N-Propylamine (Tpra) System Revisited - a New Route Involving Tpra(Center Dot+) Cation Radicals. *Journal of the American Chemical Society* **2002**, *124*, 14478-14485.
14. Choi, J. P.; Bard, A. J., Electrogenerated Chemiluminescence (Ecl) 79. Reductive-Oxidation Ecl of Tris(2,2'-Bipyridine)Ruthenium(Ii) Using Hydrogen Peroxide as a Coreactant in Ph 7.5 Phosphate Buffer Solution. *Analytica Chimica Acta* **2005**, *541*, 143-150.

15. F. M. Boldt, J. Heinze, M. Diez, J. Petersen and M. Borsch, Real-time pH microscopy down to the molecular level by combined scanning electrochemical microscopy/single-molecule fluorescence spectroscopy. *Anal. Chem.*, **2004**, *76*, 3473-3481.
16. R. Mukhopadhyay, SECM meets fluorescence microscopy. *Anal. Chem.*, **2004**, *76*, 224A-224A.
17. S. E. Salamifar and R. Y. Lai, Use of Combined Scanning Electrochemical and Fluorescence Microscopy for Detection of Reactive Oxygen Species in Prostate Cancer Cells. *Anal. Chem.*, **2013**, *85*, 9417-9421.
18. J. Kim, A. Izadyar, M. Shen, R. Ishimatsu and S. Amemiya, Ion Permeability of the Nuclear Pore Complex and Ion-Induced Macromolecular Permeation as Studied by Scanning Electrochemical and Fluorescence Microscopy. *Anal. Chem.*, **2014**, *86*, 2090-2098.
19. C. Renault, K. Marchuk, H. S. Ahn, E. J. Titus, J. Kim, K. A. Willets and A. J. Bard, Observation of Nanometer-Sized Electro-Active Defects in Insulating Layers by Fluorescence Microscopy and Electrochemistry. *Anal. Chem.*, **2015**, *87*, 5730-5737.
20. L. Guerret-Legras, J. F. Audibert, G. V. Dubacheva and F. Miomandre, Combined scanning electrochemical and fluorescence microscopies using a tetrazine as a single redox and luminescent (electrofluorochromic) probe. *Chem. Sci.*, **2018**, *9*, 5897-5905.
21. L. Guerret-Legras, J. F. Audibert, I. M. G. Ojeda, G. V. Dubacheva and F. Miomandre, SECM-fluorescence microscopy using a water-soluble electrofluorochromic dye as the redox mediator. *Electrochim. Acta*, **2019**, *305*, 370-377.
22. L.-C. Chen, W. R. Lloyd, III, C.-W. Chang, D. Sud and M.-A. Mycek, Fluorescence Lifetime Imaging Microscopy for Quantitative Biological Imaging. in *Digital Microscopy, 4th Edition*, eds. G. Sluder and D. E. Wolf, **2013**, *114*, 457-488.
23. A. Boreham, R. Brodwolf, K. Walker, R. Haag and U. Alexiev, Time-Resolved Fluorescence Spectroscopy and Fluorescence Lifetime Imaging Microscopy for Characterization of Dendritic Polymer Nanoparticles and Applications in Nanomedicine. *Molecules*, **2017**, 22.
24. M. C. Skala, K. M. Riching, A. Gendron-Fitzpatrick, J. Eickhoff, K. W. Eliceiri, J. G. White and N. Ramanujam, In vivo multiphoton microscopy of NADH and FAD redox states, fluorescence lifetimes, and cellular morphology in precancerous epithelia. *Proceedings of the National Academy of Sciences of the United States of America*, **2007**, *104*, 19494-19499.
25. R. Cao, H. Wallrabe, K. Siller, S. R. Alam and A. Periasamy, Single-cell redox states analyzed by fluorescence lifetime metrics and tryptophan FRET interaction with NAD(P)H. *Cytometry Part A*, **2019**, *95A*, 110-121.
26. F. Miomandre, E. Lepicier, S. Munteanu, O. Galangau, J. F. Audibert, R. Meallet-Renault, P. Audebert and R. B. Pansu, Electrochemical Monitoring of the Fluorescence Emission of Tetrazine and Bodipy Dyes Using Total Internal Reflection Fluorescence Microscopy Coupled to Electrochemistry. *ACS Appl. Mater. Int.*, **2011**, *3*, 690-696.
27. F. Miomandre, R. B. Pansu, J. F. Audibert, A. Guerlin and C. R. Mayer, Electrofluorochromism of a ruthenium complex investigated by time resolved TIRF microscopy coupled to an electrochemical cell. *Electrochem. Commun.*, **2012**, *20*, 83-87.
28. D. A. Buttry and F. C. Anson, ELECTROCHEMICAL CONTROL OF THE LUMINESCENT LIFETIME OF RU(BPY)32+STAR INCORPORATED IN NAFION FILMS ON GRAPHITE-ELECTRODES. *J. Am. Chem. Soc.*, **1982**, *104*, 4824-4829.
29. G. Clavier and P. Audebert, s-Tetrazines as Building Blocks for New Functional Molecules and Molecular Materials. *Chem. Rev.*, **2010**, *110*, 3299-3314.
30. P. Audebert, F. Miomandre, G. Clavier, M. C. Vernieres, S. Badre and R. Meallet-Renault, Synthesis and properties of new tetrazines substituted by heteroatoms: Towards the world's smallest organic fluorophores. *Chem.Eur. J.*, **2005**, *11*, 5667-5673.
31. Gaussian 16, Revision B.01, M. J. Frisch, G. W. Trucks, H. B. Schlegel, G. E. Scuseria, M. A. Robb, J. R. Cheeseman, G. Scalmani, V. Barone, G. A. Petersson, H. Nakatsuji, X. Li, M. Caricato, A. V. Marenich, J. Bloino, B. G. Janesko, R. Gomperts, B. Mennucci, H. P. Hratchian, J. V. Ortiz, A. F. Izmaylov, J. L. Sonnenberg, D. Williams-Young, F. Ding, F. Lipparini, F. Egidi, J. Goings, B. Peng, A. Petrone, T. Henderson, D. Ranasinghe, V. G. Zakrzewski, J. Gao, N. Rega, G. Zheng, W. Liang,

M. Hada, M. Ehara, K. Toyota, R. Fukuda, J. Hasegawa, M. Ishida, T. Nakajima, Y. Honda, O. Kitao, H. Nakai, T. Vreven, K. Throssell, J. A. Montgomery, Jr., J. E. Peralta, F. Ogliaro, M. J. Bearpark, J. J. Heyd, E. N. Brothers, K. N. Kudin, V. N. Staroverov, T. A. Keith, R. Kobayashi, J. Normand, K. Raghavachari, A. P. Rendell, J. C. Burant, S. S. Iyengar, J. Tomasi, M. Cossi, J. M. Millam, M. Klene, C. Adamo, R. Cammi, J. W. Ochterski, R. L. Martin, K. Morokuma, O. Farkas, J. B. Foresman, and D. J. Fox, Gaussian, Inc., Wallingford CT, **2016**.

32. M. Tsushima, T. Ushizaka and N. Ohta, Time-resolved measurement system of electrofluorescence spectra. *Rev. Sci. Instrum.*, **2004**, *75*, 479-485.
33. Wahl, M., Time-correlated single photon counting. **2014**. *Technical Note* 1–14.
34. Eaton, D.F., Recommended methods for fluorescence decay analysis. Pure and applied chemistry **1990** 62, 1631–1648.
35. Hall, P., Selinger, B.,. Better estimates of exponential decay parameters. *J. Phys. Chem.* **1981** *85*, 2941–2946.
36. Köllner, M., Wolfrum, J. How many photons are necessary for fluorescence-lifetime measurements? Chemical Physics Letters **1992** 200, 199–204.
37. A. J. Bard and Faulkner, *Electrochemical Methods : Fundamentals and Applications (2nd edition)*, Chapter 5, Wiley, New York, **2000**.
38. M. V. Smoluchowski, Versuch einer mathematischen Theorie der Koagulationskinetik kolloider Lösungen. *Zeitschrift für physikalische Chemie*, **1918**, *92*, 129-168.
39. C.S. Lunardi, J.B.S. Bonilha, A.C. Tedesco, Stern–Volmer quenching and binding constants of 10-alkyl-9(10H)-acridone probes in SDS and BSA. *J. Lumin.*, **2002**, *99*, 61-71.

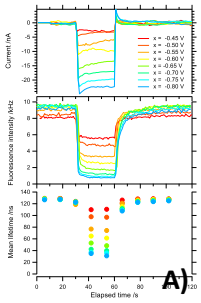

A)

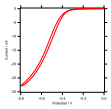

D)

B)

C)

Figure 1: Current (A), fluorescence intensity (B) and fluorescence lifetime (C) vs. time at various potentials (same color codes for all curves) for a fixed position of the Scanning Electrochemical Microscope tip (30 µm above the substrate). The potential varies from 0 V (0-30 s) to the indicated value (30-60 s) and back to 0 V (60-120 s) and refer to the CV recorded at the microelectrode tip at 50 mV/s (D).

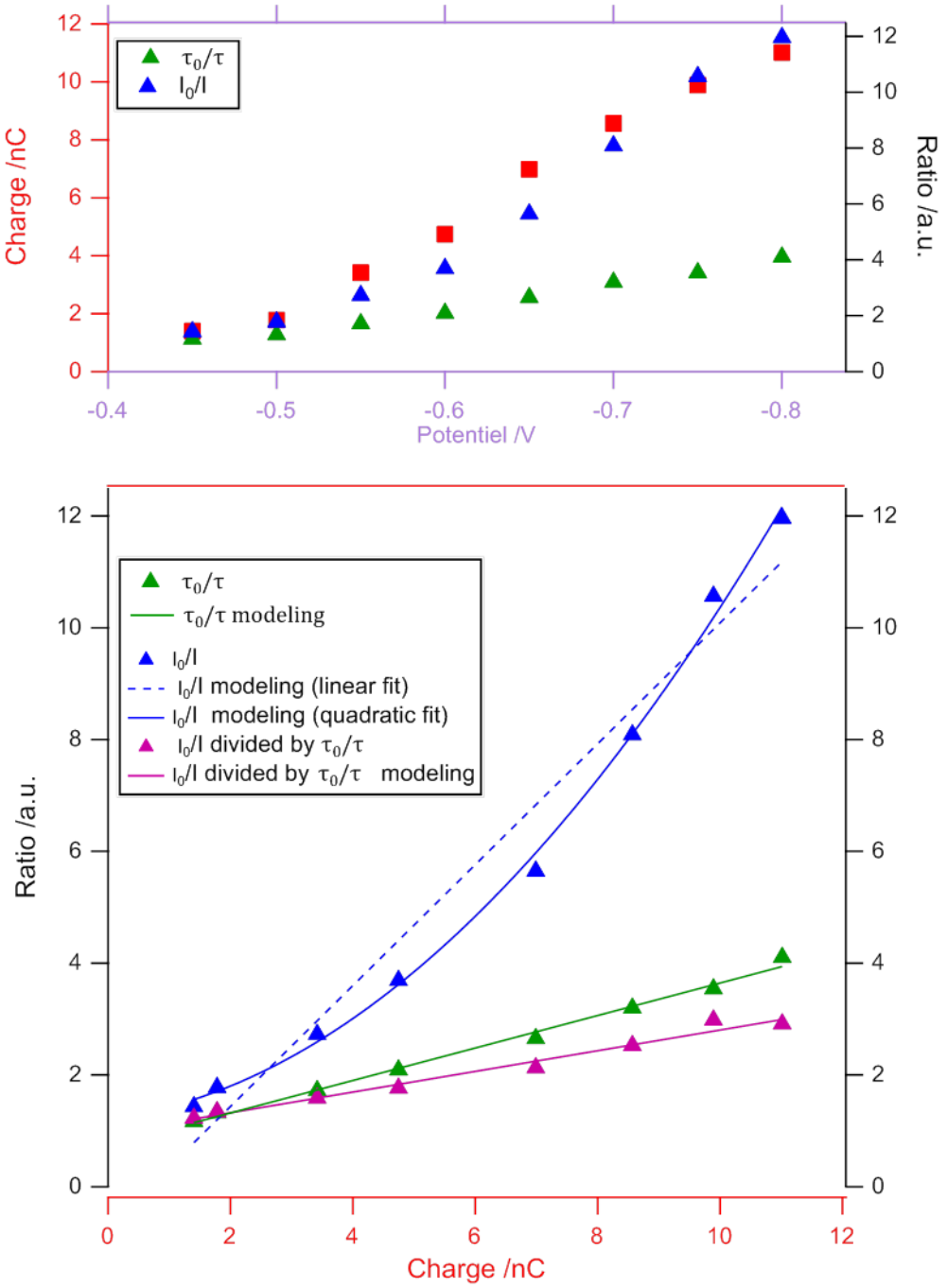

Figure 2: Coulombic charge measured by integrating current from 30 to 60 s (red), fluorescence intensity I (blue) and fluorescence lifetime T (green) ratios vs. potential (top panel) on glass substrate. Ratios are measured between the oxidized state and the given potential.

Same fluorescence intensity and lifetime ratios vs. charge (bottom panel). Full line shows the fitting of experimental data.

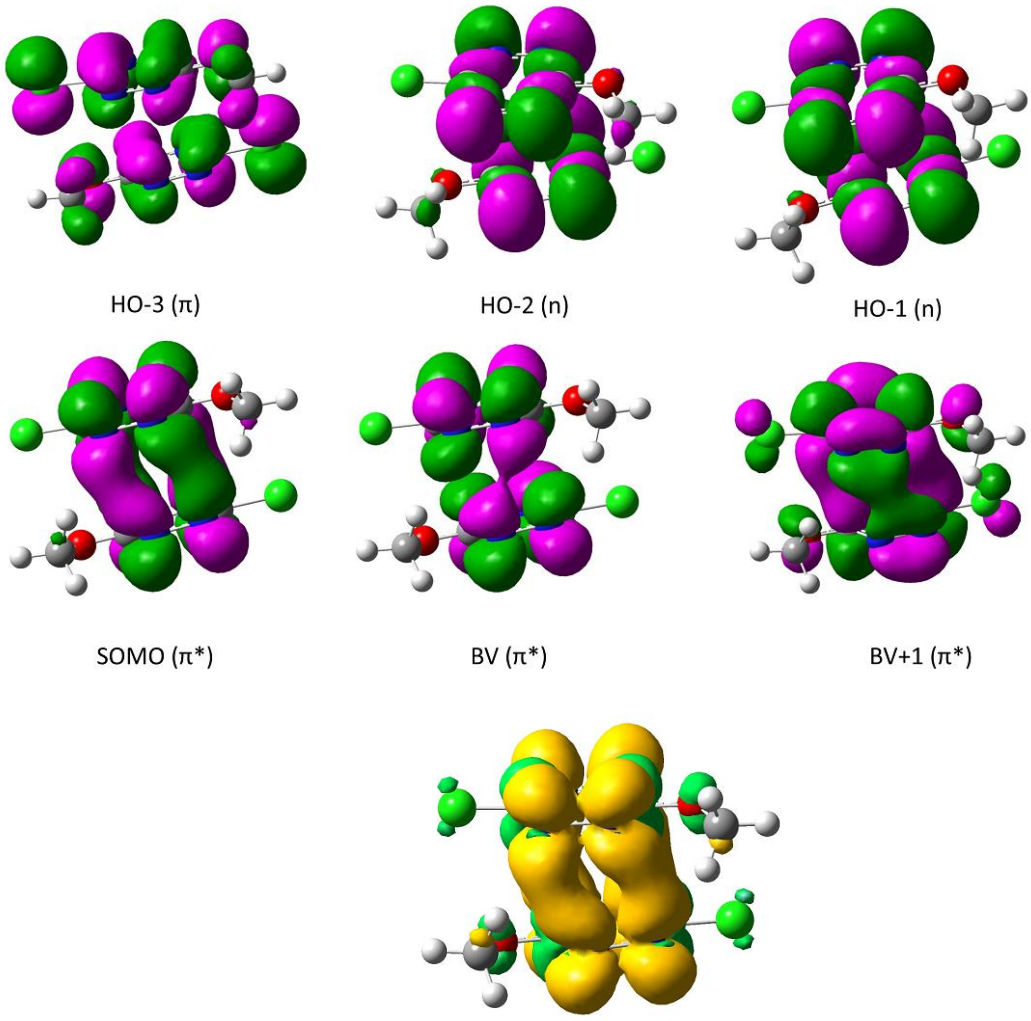

Figure 3: Frontier molecular orbitals (top) and spin density (bottom) for the complex formed by neutral chloromethoxytetrazine and its anion radical ($Tz,Tz^{\bullet-}$) calculated with APFD theory.

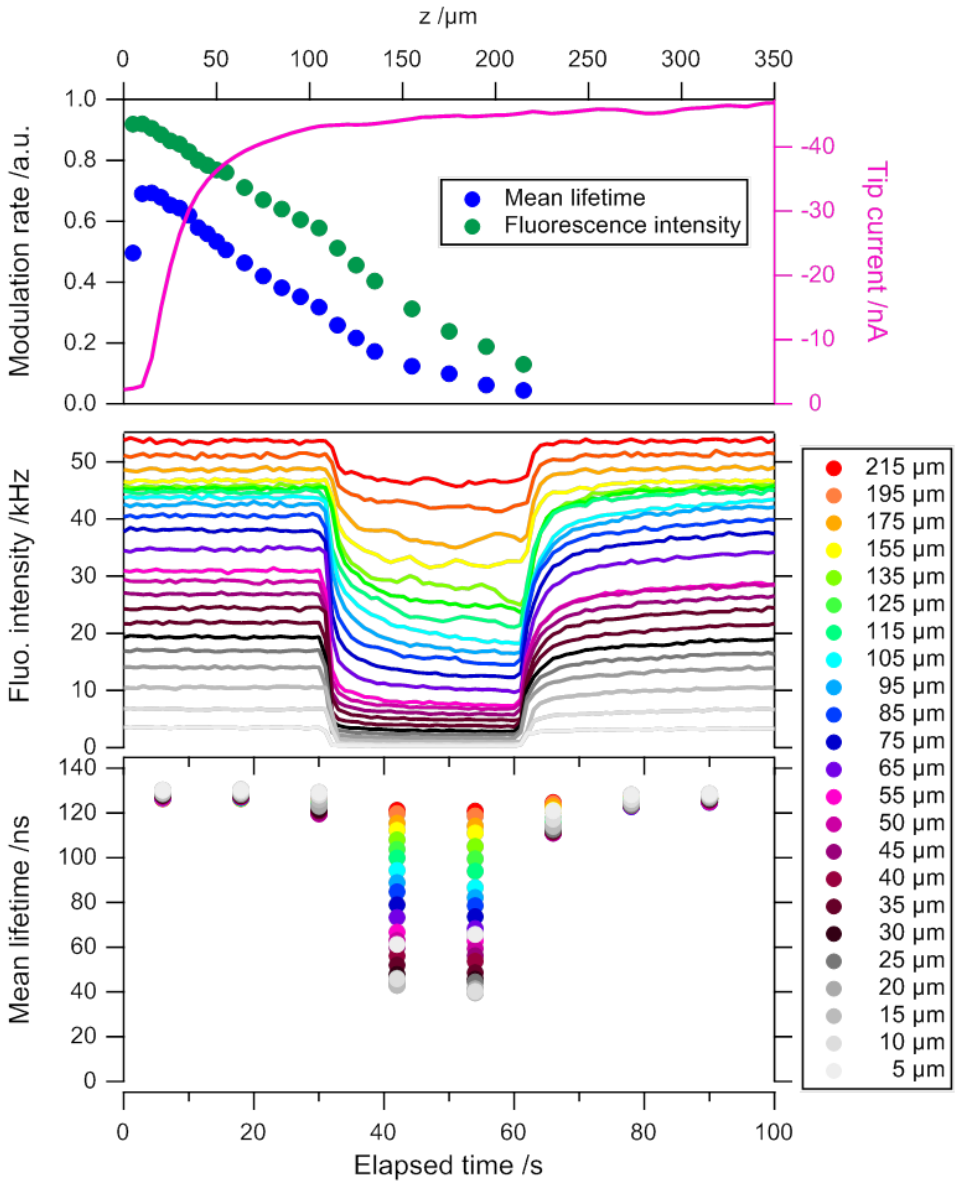

Figure 4: Current (top panel), fluorescence intensity (medium panel) and fluorescence lifetime (bottom panel) vs. time at various tip positions (same color codes for all curves) for a potential signal of: 0 V (0-30 s); -0.7V (30-60 s); 0 V (60-100 s).

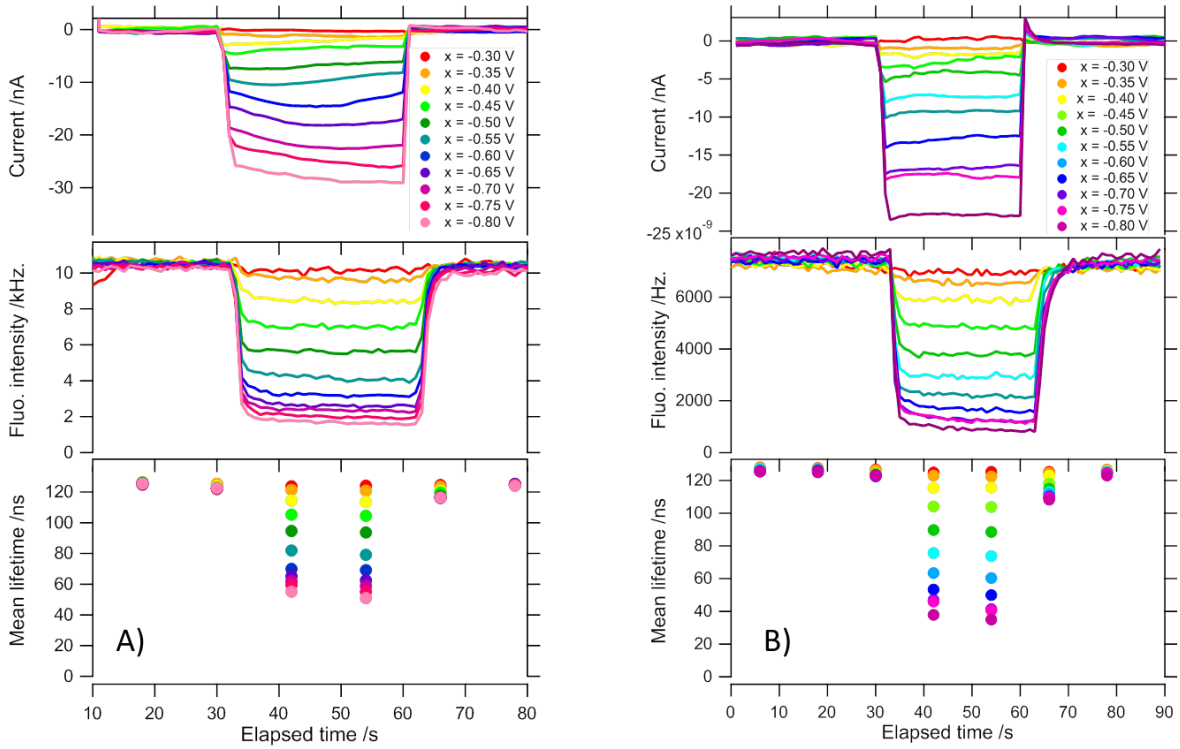

Figure 5: Electrochemical current (top panel), fluorescence intensity (medium panel) and fluorescence lifetime (bottom panel) vs. time at various potentials (same color codes for all curves) for a fixed position of the tip (30 µm) above the ITO substrate under open circuit (A) or polarized at -0.23 V (B). The potential varies from 0 V (0-30 s) to the indicated value x V (30-60 s) and back to 0 V (60-120 s).

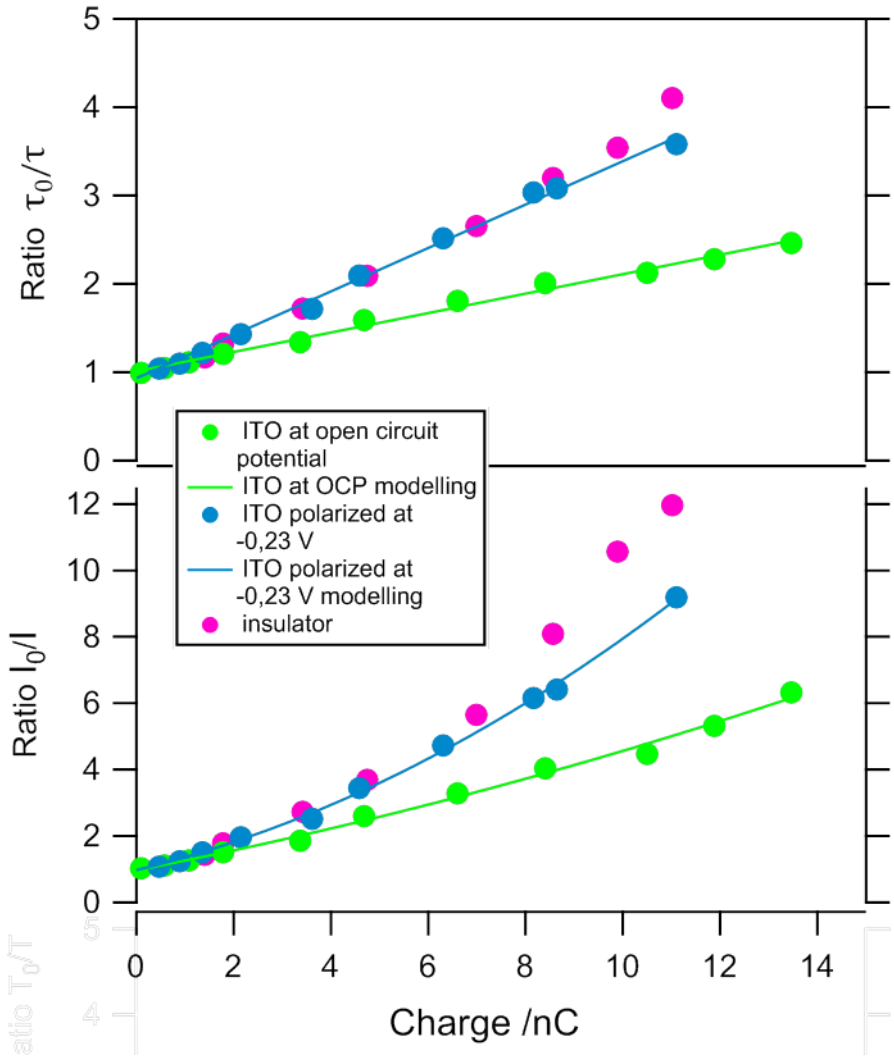

Figure 6: Luminescence intensity and luminescence lifetime ratios vs. charge on glass (pink), ITO at open circuit (green), ITO polarized at -0.23 V (blue). Full lines are the fitting curves, dots are the experimental points.

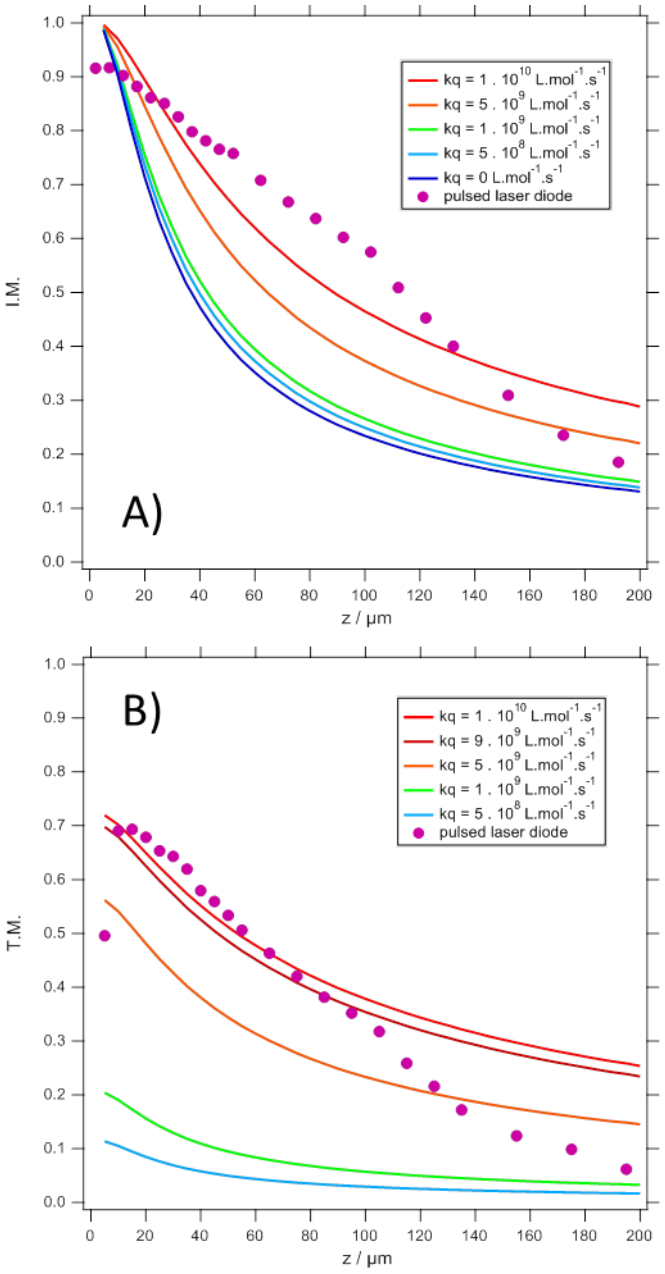

Figure 7: Simulation of the modulation amplitude of luminescence intensity (A) and lifetime (B) vs. tip position for various values of the quenching rate constant (full lines). Experimental data are shown by dots.